MODELING AND ANALYSIS

Nested control loop design for differential boost inverter using generalized averaged model in photovoltaic applications

Ali Amirparast [ID] | Hossein Gholizade-narm

Faculty of Electrical Engineering and Robotics, Shahrood University of Technology, Shahrood, Iran

Correspondence
Ali Amirparast, Faculty of Electrical Engineering and Robotics, Shahrood University of Technology, Shahrood, Iran.
Email: ali.amirparast@shahroodut.ac.ir

Abstract

To use photovoltaic energy, voltage source inverters are playing an important role. The most of local AC loads such as AC motors need higher voltage than solar panel output voltage. Differential boost inverter produces an AC voltage that is greater than the DC input voltage in a single power stage. This inverter consists of two DC-DC bilateral boost converters in which work via time-variant duty cycles to produce sinusoidal voltage, and this feature causes complexity in control design. To deal with this complexity, new modeling so-called generalized averaged model is used to achieve a linear time-invariant model. In this paper, a nested control loop is designed. This control strategy consists of two control loops in which the inner loop is designed by linear quadratic regulator theory to displace poles in proper location and the second loop uses a PI-PR controller to track desired voltage and reject disturbances. To evaluate the proposed control method, the sliding mode controller is applied and compared as well. As shown by simulations, the proposed control strategy has more reliable performance and provides higher robustness in comparison with sliding mode control technique in rigid situations such as dealing with nonlinear load, parameters values changes, and external disturbances.

KEYWORDS

boost inverter, generalized averaged model, linear quadratic regulator, PI-PR, renewable energies

1 | INTRODUCTION

The negative environmental aspects of using fossil fuel to produce electricity highlight the role of renewable energy sources in this subject. One of the high-efficiency renewable energy sources to generate electricity is photovoltaic energy.[1,2] To transmit photovoltaic energy into the power grid, using boost inverters are inevitable.[3] The differential boost inverter (DBI) consists of two DC-DC boost converter. Each boost converter produces DC-biased sinusoidal AC voltage in its output due to the time-varying duty cycle

as a consequence; the output voltage of DBI is a pure AC voltage and greater than DC input voltage.[4] The idea of controlling the phase shift between two boost DC-DC converters to make a DC-AC inverter is also provided by the theory of phase-modulated inverters, which is presented and analyzed in.[5] DBI has many advantages. The most important advantage is generating AC voltage which has a higher amplitude than the input voltage in just one power stage. The reduced number of switches and quality of output voltage in comparison with other boost inverters are other advantages that have been expressed in.[4,6]

To control this inverter, the control of each two boost converter is required. Although the boost converters are not easy to control, several methods based on linear small-signal model have been introduced in literature.[7,8] These methods are not suitable to control the individual boosts of the inverter due to time-varying operation points in the small-signal model.[9]

A conventional method to control boost converters is sliding mode control (SMC). This technique can deal with variable operation point conditions and also provides a good steady-state result.[6,10,11] However, this control method has some drawbacks such as required complex theory, variable switching frequency, and instability in dealing with some external disturbances.[12]

This paper uses a new modeling method so-called generalized averaged model (GAM) which can extract a LTI small-signal model from nonlinear switched model with large variation of operation points. In the following, a nested control loop strategy for the boost inverter is proposed, in which, each boost converter is controlled by means of a double-loop control scheme that consists of an optimal state feedback control loop as inner loop and a proportional integral-proportional resonance (PI-PR) controller as outer loop. The inner loop provides enough damping to improve transient state of output voltage and outer loop objects are aimed at desired voltage tracking and disturbance rejection. As it will be shown through this paper, the control of the output voltage by means of two nested loop makes possible to cope with special situations that cannot be tackled by the SMC, such as connecting to nonlinear load, parameters values changes, and external disturbances. The paper is organized as follows: system description is reviewed in Section 2; GAM method is expressed in Section 3; the nested control loop is designed in Section 4; simulation results and comparison with sliding mode are studied in Section 5; and finally, conclusion is given in Section 6.

2 | SYSTEM DESCRIPTION AND PROBLEM STATEMENT

Figure 1 shows the block diagram of a single phase DBI. This inverter consists of two boost converters, and the output of converters is connected differentially.[4]

In this inverter, Q_1 and Q_2 are left converter switches which operate via duty cycles D and $1-D$, respectively, and in the other side, Q_3 and Q_4 are right converter switches which work via duty cycles D' and $1-D'$, respectively. $C_{1,2}$ are capacitors and $L_{1,2}$ are inductors of DBI. In the description of the operation of the converters, it is assumed each converter operates in continuous conduction mode (CCM). Each boost converter has two operation modes in one cycle. For example,

in left converter when the switch Q_1 is on and Q_2 is off, current i_1 rises and capacitor C_1 supplies energy to the output. In the next mode, once the switch Q_1 is off and Q_2 is on, current i_1 flows through capacitor C_1 and the output stage. The current i_1 decreases while capacitor C1 is recharged. The main feature of DBI is each boost converter produces AC voltage along with DC voltage in its output due to specific time-variant duty cycles which results a sinusoid AC voltage over the load. Moreover, this inverter has a hidden LCL filter in its circuit in which attenuates higher harmonics.[13] Figure 2 shows the circuit diagram of DBI.

According to Figure 2, the switched model equations for the resistive load can be achieved as follows:

$$
\begin{aligned}
L_1 \dot{i}_1 &= V_{\text{in}} - D v_1 \\
C_1 \dot{v}_1 &= D i_1 - \frac{(v_1 - v_2)}{R} \\
L_2 \dot{i}_2 &= V_{\text{in}} - D' v_1 \\
C_2 \dot{v}_2 &= D' i_2 + \frac{(v_1 - v_2)}{R}
\end{aligned}
\tag{1}
$$

In Equation (1), i_1 and i_2 are inductor currents; v_1 and v_2 are capacitor voltages, and V_{in} is output voltage of photovoltaic panel In the following, by considering switched model equations in their steady-state form ($\dot{i}_{1,2} = 0$, $\dot{V}_{1,2} = 0$) and solve the equations, the steady-state duty cycles can be achieved approximately as Equation (2).

$$
\begin{aligned}
D(t) &= \frac{1}{\alpha + \beta \sin(\omega t)} \\
D'(t) &= \frac{1}{\alpha - \beta \sin(\omega t)}
\end{aligned}
\tag{2}
$$

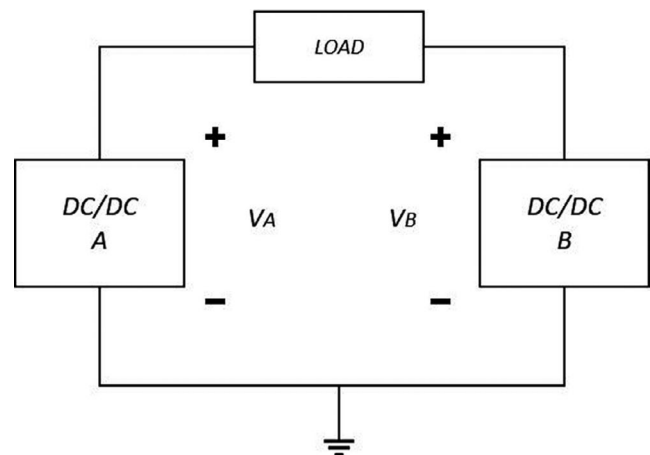In Equation (2), α and β can be achieved based on desired output voltage (V_o) as Equation (3).
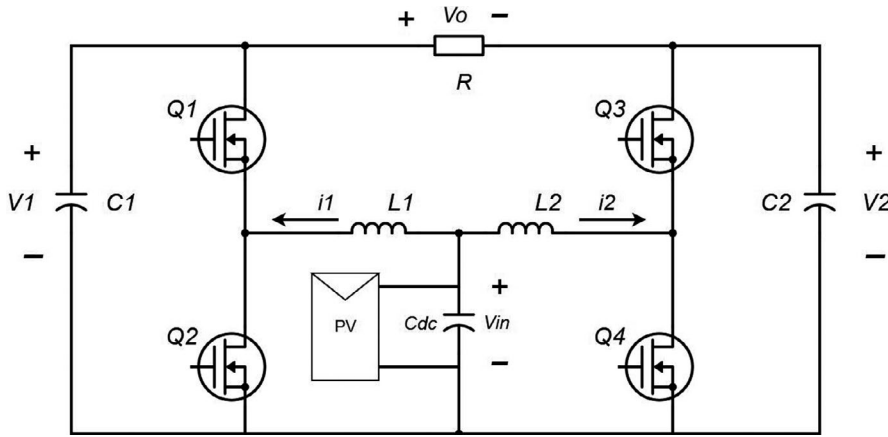

FIGURE 1   The block diagram of DBI

FIGURE 2 The circuit diagram of DBI

$$\alpha = \frac{V_1 + V_2}{2V_{\text{in}}}$$

$$\beta = \frac{|V_1 - V_2|}{2V_{\text{in}}}$$

$$V_1 = V_{\text{dc}} + V_{\text{ac}}\sin(\omega t)$$

$$V_2 = V_{\text{dc}} - V_{\text{ac}}\sin(\omega t) \tag{3}$$

$$V_{\text{ac}} = \frac{|V_o|}{2}$$

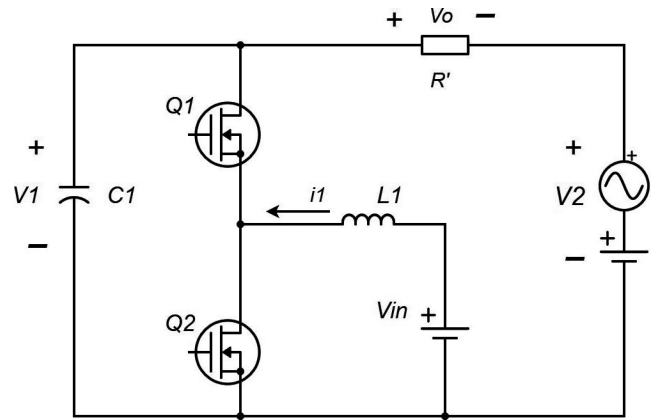$$V_{\text{dc}} = \frac{|V_o| + 2V_{\text{in}}}{2}$$

$$\omega = 2\pi f$$

FIGURE 3 The half circuit diagram of DBI

For example, to achieve $V_o = 311\sin(\omega t)$, by consideration $V_i n = 100$, the parameters of Equation (2) are $\alpha = 2.55$ and $\beta = 1.55$. One of the biggest problems of this inverter is lack of enough damping in which results instability in dealing with significant parameters values changes or some external disturbances. In this paper, to solve mentioned problem, an optimal state feedback controller is used as active damping which can be computed via LQR theory. Moreover, this technique provides 60 degree phase margin and almost infinity gain margin. To use this technique, system equations should be linearized. Due to periodic time-varying operation points, the system with Equation (1) will be turned into a periodic linear time-varying (LTV) system after linearization. To achieve optimal gains via LQR for a periodic LTV system, the periodic Riccati differential equations (PRDE) should be solved which needs complicated algorithms.[14] The GAM method is used to extract a linear time-invariant (LTI) system equation from Equation (1) which leads to solving a simple algebraic Riccati equations (ARE) for achieving optimal gains. In addition, the PI-PR controller is used for tracking voltage reference. For simplicity and without losing generality, to model and control this inverter, the half circuit of DBI is considered. It should be noted that the designed control loops for two converters (in terms of numerical values) are exactly the same.[6,9]

In Figure 3, the half circuit of DBI is illustrated which V_2 is steady-state voltage of right boost converter and $R' = \frac{R}{2}$.

3 | GENERALIZED AVERAGED MODEL

The GAM is based on the waveform illustration using the complex Fourier series. Two substantial rules are expressed according to complex Fourier series equations.[15,16]

$$\frac{d}{dt}\langle x \rangle_k(t) = \langle \frac{d}{dt}x \rangle(t) - jk\omega\langle x \rangle_k(t)$$

$$\langle x \cdot y \rangle_k(t) = \sum_i \langle x \rangle_{k-i}(t) \cdot \langle y \rangle_i(t) \tag{4}$$

where ω is the base frequency and $\langle x \rangle_k$ is the moving average of k_{th} harmonic coefficient.[15,16] According to system operation, AC and DC voltages are dropped over the load by each boost converter. Therefore, zero-order and first-order harmonics of the switched model are considered. Moreover, considering the number of harmonic's orders of the switched model for GAM is a compromise between accuracy and simplicity of the

harmonic model. According to the rules (4), GAM equations are expressed for the inverter with the resistive load as follows:

$$L_1 \frac{d}{dt} \langle i_1 \rangle_0 = \langle V_{in} \rangle_0 - \langle Dv_1 \rangle_0$$

$$L_1 \frac{d}{dt} \langle i_1 \rangle_1 = \langle V_{in} \rangle_1 - \langle Dv_1 \rangle_1 - jL_1 \omega \langle i_1 \rangle_1$$

$$C_1 \frac{d}{dt} \langle v_1 \rangle_0 = \langle Di_1 \rangle_0 - \frac{(\langle v_1 \rangle_0 - \langle v_2 \rangle_0)}{R} \tag{5}$$

$$C_1 \frac{d}{dt} \langle v_1 \rangle_1 = \langle Di_1 \rangle_1 - \frac{(\langle v_1 \rangle_1 - \langle v_2 \rangle_1)}{R} - jC_1 \omega \langle v_1 \rangle_1$$

For simplicity, we define variables (6):

$$\langle V_{in} \rangle_0 = V_{in}$$
$$\langle V_{in} \rangle_1 = 0$$
$$\langle i_1 \rangle_0 = x_1$$
$$\langle i_1 \rangle_1 = x_2 + jx_3$$
$$\langle v_1 \rangle_0 = x_4$$
$$\langle v_1 \rangle_1 = x_5 + jx_6 \tag{6}$$
$$\langle v_2 \rangle_0 = x_{10} = M$$
$$\langle v_2 \rangle_1 = x_{11} + jx_{12} = 0 + j\frac{N}{2}$$
$$\langle D_1 \rangle_0 = u_1$$
$$\langle D_1 \rangle_1 = u_2 + ju_3$$

by using variables (6), the Equation (5) are turned into final form of GAM:

$$L_1 \dot{x}_1 = V_{in} - 2(x_5 u_2 + x_6 u_3) - u_1 x_4$$

$$L_1 \dot{x}_2 = L_1 \omega x_3 - x_4 u_2 - u_1 x_5$$

$$L_1 \dot{x}_3 = -L_1 \omega x_2 - x_4 u_3 - u_1 x_6$$

$$C_1 \dot{x}_4 = 2(x_2 u_2 + x_3 u_3) - \frac{1}{R'}(x_4 - x_{10}) + u_1 x_1 \tag{7}$$

$$C_1 \dot{x}_5 = C_1 \omega x_6 + x_1 u_2 - \frac{1}{R'}(x_5 - x_{11}) + u_1 x_2$$

$$C_1 \dot{x}_6 = -C_1 \omega x6 + x_1 u_3 - \frac{1}{R'}(x_6 - x_{12}) + u_1 x_3$$

In Equation (7), x_i $(i = 1 \dots 6)$ and u_i $(i = 1 \dots 3)$ are state variables and control inputs of GAM, respectively.

3.1 | Linearization

According to the GAM method, zero and first harmonic order of switched model state variables is considered. Therefore, the DBI is linearized around harmonic coefficients of switched model operation points.

To design the nested control loop, the nonlinear dynamics Equation (7) is linearized around the harmonic operation

point using Taylor expansion. It is assumed that each harmonic coefficient has a small variation around the operation point and steady-state value.

$$\mathbf{x} = \overbrace{\mathbf{X}}^{\text{steady state value}} + \overbrace{\tilde{\mathbf{x}}}^{\text{small variation}} \tag{8}$$

$$\mathbf{u} = \mathbf{U} + \tilde{\mathbf{u}}$$

Assuming that $\|\mathbf{X}\| \gg \|\tilde{\mathbf{x}}\|$ linearization of Equation (7) is shown in matrix form (9). In Equation (9), B_d is input matrix of disturbance (d) which can be entered to system.

$$\dot{\tilde{\mathbf{x}}} = A\tilde{\mathbf{x}} + B\tilde{\mathbf{u}} + \overbrace{B_d d}^{\text{External disturbance}} \tag{9}$$

$$\mathbf{y} = C\tilde{\mathbf{x}} + D\tilde{\mathbf{u}}$$

where

$$A = \begin{pmatrix} 0 & 0 & 0 & \frac{-U_1}{L_1} & \frac{-2U_2}{L_1} & \frac{-2U_3}{L_1} \\ 0 & 0 & \omega & \frac{-U_2}{L_1} & \frac{-U_1}{L_1} & 0 \\ 0 & -\omega & 0 & \frac{-U_3}{L_1} & 0 & \frac{-U_1}{L_1} \\ \frac{U_1}{C_1} & \frac{2U_2}{C_1} & \frac{2U_3}{C_1} & \frac{-1}{RC} & 0 & 0 \\ \frac{U_2}{C_1} & \frac{U_1}{C_1} & 0 & 0 & \frac{-1}{RC} & \omega \\ \frac{U_3}{C_1} & 0 & \frac{U_1}{C_1} & 0 & -\omega & \frac{-1}{RC} \end{pmatrix}.$$

$$B = \begin{pmatrix} \frac{-X_4}{L_1} & \frac{-2X_5}{L_1} & \frac{-2X_6}{L_1} \\ \frac{-X_5}{L_1} & \frac{-X_4}{L_1} & 0 \\ \frac{-X_6}{L_1} & 0 & \frac{-X_4}{L_1} \\ \frac{X_1}{C_1} & \frac{2X_2}{C_1} & \frac{2X_3}{C_1} \\ \frac{X_2}{C_1} & \frac{X_1}{C_1} & 0 \\ \frac{X_3}{C_1} & 0 & \frac{X_1}{C_1} \end{pmatrix}.$$

$$C = \begin{pmatrix} 0 & 0 & 0 & 1 & 0 & 0 \\ 0 & 0 & 0 & 0 & 1 & 0 \\ 0 & 0 & 0 & 0 & 0 & 1 \end{pmatrix}.$$

$$D = 0.$$

$$B_d = \begin{pmatrix} d_1 & d_2 & \dots & d_6 \end{pmatrix}^T.$$

3.2 | Harmonic extraction

The approximated relation between AC part of real-time-varying state variable signals and harmonic coefficients is expressed based on complex Fourier series equation as Equation (10).[16]

$$\tilde{i}_1(t) = 2\left(\tilde{x}_2 \cdot \cos(\omega t) - \tilde{x}_3 \sin(\omega t)\right)$$
$$\tilde{v}_1(t) = 2\left(\tilde{x}_5 \cdot \cos(\omega t) - \tilde{x}_6 \sin(\omega t)\right) \quad (10)$$

To extract harmonic coefficients $\tilde{x}_2$ and $\tilde{x}_5$ from real-time-varying voltage and current signals, the voltage and current signals are multiplied by $\cos(\omega t)$. Similarly, to extract $\tilde{x}_3$ and $\tilde{x}_6$, current and voltage are multiplied by $\sin(\omega t)$, respectively. After performing an elementary trigonometric transform, the following expression is reached as Equations (11) and (12).

$$\tilde{i}_1(t) \cdot \cos(\omega t) = \overbrace{\tilde{x}_2}^{\text{DC Part}} + \overbrace{\tilde{x}_2 \cdot \cos(2\omega t) - \tilde{x}_3 \sin(2\omega t)}^{\text{AC Part}} \quad (11)$$
$$\tilde{v}_1(t) \cdot \cos(\omega t) = \tilde{x}_5 + \tilde{x}_5 \cdot \cos(2\omega t) - \tilde{x}_6 \sin(2\omega t)$$

$$\tilde{i}_1(t) \cdot \sin(\omega t) = \overbrace{\tilde{x}_3}^{\text{DC Part}} - \overbrace{\tilde{x}_3 \cdot \cos(2\omega t) + \tilde{x}_2 \sin(2\omega t)}^{\text{AC Part}} \quad (12)$$
$$\tilde{v}_1(t) \cdot \sin(\omega t) = \tilde{x}_6 - \tilde{x}_6 \cdot \cos(2\omega t) + \tilde{x}_5 \sin(2\omega t)$$

where two distinct components have been identified: a DC one and a 2ω-pulsation AC component in both equations. To extract DC part, it is sufficient to apply a low-pass filter to eliminate the AC components without significantly affecting the dynamic of the continuous components (eg, by using conveniently sized Butterworth filters).[16] In addition, to extract zero-order harmonic coefficients $\tilde{x}_1$ and $\tilde{x}_4$ from real-time-varying signals, simply a low-passed filter can be used. To study the transient behavior of the system more precisely, the step response of the linearized GAM is shown in Figure 4. The alternative output voltage is considered $vo = 311 \sin(100\Pi t)$. Moreover, according to the DC input voltage and steady-state capacitor voltage values, the parameters of steady-state duty cycles (2) are computed as ($\alpha = 2.55$ and $\beta = 1.55$).

One can see from Figure 4 that the system does not have enough damping and it has extreme oscillations in its transient state. In the next section, an optimal state feedback controller is designed using the LQR method as the inner control loop and a PI-PR controller in the outer control loop to improve overall behavior (transient-state and steady-state), desired voltage tracking. and disturbance rejection.

4 | CONTROL DESIGN

In this section, the controller design objects are aimed at increasing damping, reference voltage tracking, and closed-loop stability. To design controller, controllability and the relative gain array (RGA) matrices are computed as follows:

$$\text{rank}\left(\varphi_c = \begin{bmatrix} B & AB & A^2B & \dots & A^5B \end{bmatrix}\right) = 6 \quad (13)$$

$$\text{RGA} = \begin{pmatrix} 2.078 & 1.18^{-6} & -1.07 \\ 1.82^{-6} & 1 & 4.89^{-6} \\ -1.07 & 4.96^{-6} & 2.07 \end{pmatrix} \quad (14)$$

According to (13), the system is controllable. Moreover, all of the elements on the main diagonal of RGA matrix (14) are positive which means control inputs can control outputs peer-to-peer.[17]

4.1 | Inner-loop design

As can be seen in Figure 4, lack of enough damping is one of the biggest problems in this inverter. One of the simplest solutions to solve this problem is adding resistances to inductors but it has some disadvantages such as power loss. Therefore, a better solution to this problem is using active damping as state feedback controller in the inner loop which is designed via LQR technique.

The aim of LQR is finding a control law that minimizes quadratic performance index (15).[18]

$$J = \frac{1}{2}\int_0^\infty \left[\tilde{X}^T Q \tilde{X} + \tilde{U}^T R \tilde{U}\right] dt \quad (15)$$

In (15), Q and R are weighted matrices, $\tilde{X}$ and $\tilde{U}$ are harmonics coefficients of state variables vector of the system and control inputs, respectively. According to state space representation of closed-loop system (9), LQR technique with performance index (15) cannot be used as a solution to achieve optimal gains due to disturbance term. Therefore, to solve LQR problem in this case, an operator $\Delta_d(D_d) = det(D_d I - A_d)$ is defined where D_d is differentiating operator, I is identity matric, and A_d is state matrix of disturbance.[19] By applying defined operator to both sides of Equation (9), $\Delta_d(D_d).d = 0$ and state space equation of closed-loop system is changed to Equation (16).[19]

$$\dot{\tilde{Z}} = A\tilde{Z} + B\tilde{V}$$
$$Y = C\tilde{Z} + D\tilde{V} \quad (16)$$

where pseudo state vector $\tilde{Z}$ and pseudo input $\tilde{V}$ are $\tilde{Z} = \Delta_d(D_d) \cdot \tilde{X}$ and $\tilde{V} = \Delta_d(D_d) \cdot \tilde{U}$, respectively. The Equation (17) shows a standard state feedback law without disturbance signal. Moreover, the pair (A, B) is stabilizable. Therefore, for any $Q = H^T H$ that makes (H, A) detectable, there

FIGURE 4   Open-loop step responses
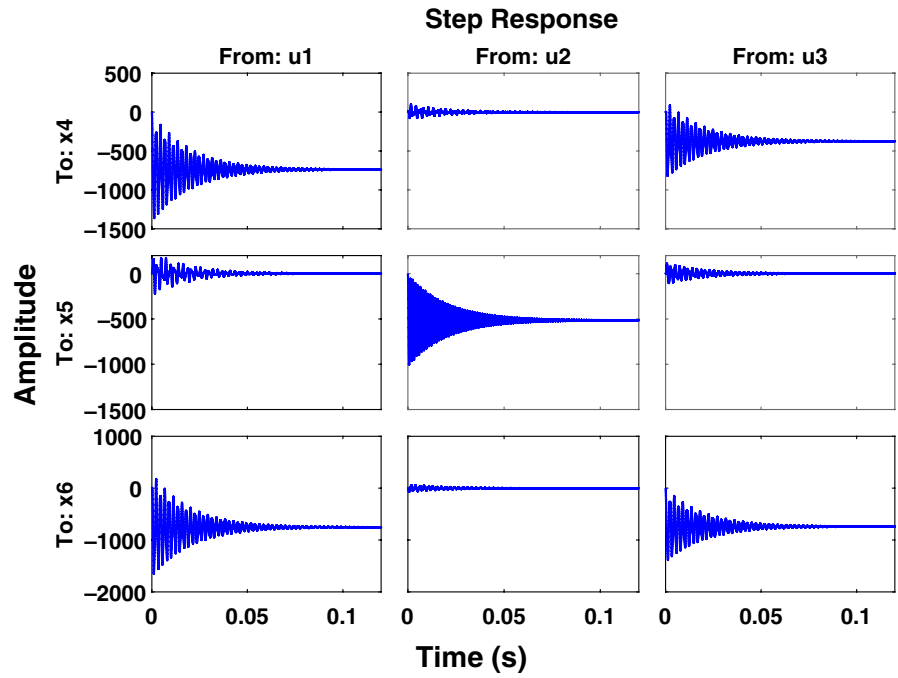
exists a solution to solve LQR problem by consideration of new performance index (18).

$$\tilde{V} = -K.\tilde{Z} \qquad (17)$$

$$J = \frac{1}{2} \int_0^\infty \left[\tilde{\mathbf{Z}}^T Q \tilde{\mathbf{Z}} + \tilde{\mathbf{V}}^T R \tilde{\mathbf{V}} \right] dt \qquad (18)$$

In this study, matrix Q is considered diagonal ($Q = diag(q)$) and q is a scalar which determines state variable weights in Q matrix. To choose q properly, poles (eigenvalues) movement must be considered. The poles movement of inner loop by changing main diagonal elements of Q ($q = 10^{-10}$ to $q = 10^{-5}$) is shown in Figure 5. According to the poles movement of the inner loop, appropriate places of poles are considered between −4000 and −4500 in the real axis. For pole placement in desired place q is computed as $\gamma \cdot 10^{-6}$.

By consideration of $\gamma = 1.5$ and $R = I$, step response of inner loop is shown in Figure 6.

As can be seen in Figure 6, the extreme oscillations are eliminated and transient state is improved as well. According to the GAM method, the main system is divided into two AC and DC subsystem. Thereby, the designed control signal should be used by Equation (19) which can be extracted from Fourier basic equations approximately. In other words, zero- and first-order harmonic of steady-state duty cycle ($D(t)$) are modified by the designed controller signal.

$$d(t) = \tilde{u}_1 + 2\left(\tilde{u}_2 \cdot \cos(\omega t) - \tilde{u}_3 \sin(\omega t) \right) \qquad (19)$$
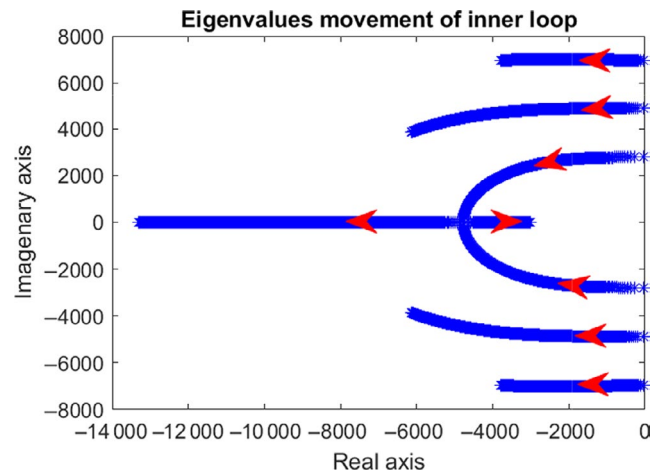

FIGURE 5   POLES movement by changing $q = 10^{-10}$ to $q = 10^{-5}$

4.2 | Outer loop design

The main purpose of the design of the outer control loop is desired voltage tracking in the presence of disturbance in input voltage. A PI-PR controller with transfer function (20) is designed to track the desired output voltage in two frequency $(0, \omega)$ with respect to DC and AC part of reference voltage.[20] Poles and zeroes of the closed-loop system are shown in Figure 7.

$$C(s) = K_p + \frac{K_i}{S} + \frac{K_r.S}{S^2 + \omega^2} \qquad (20)$$
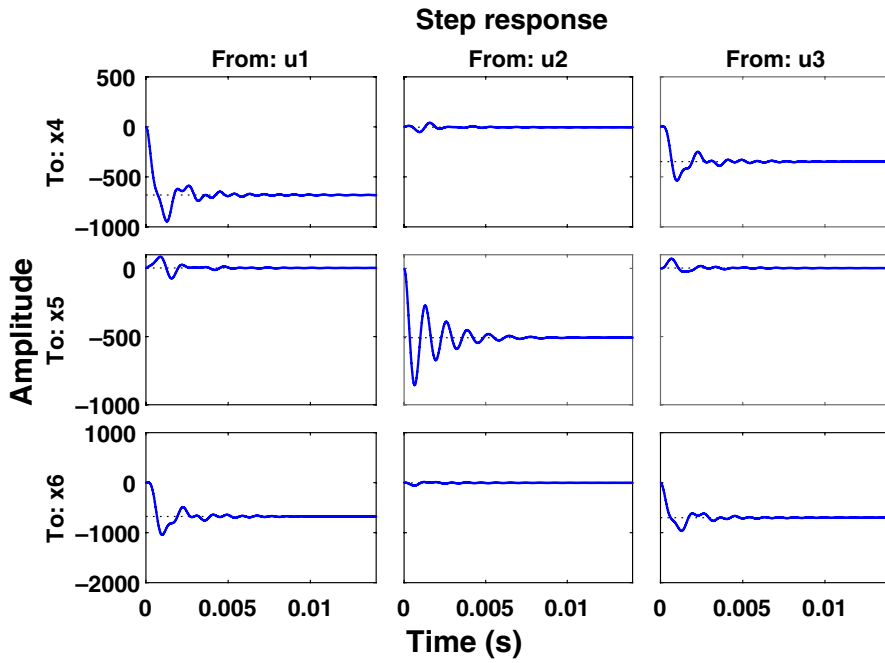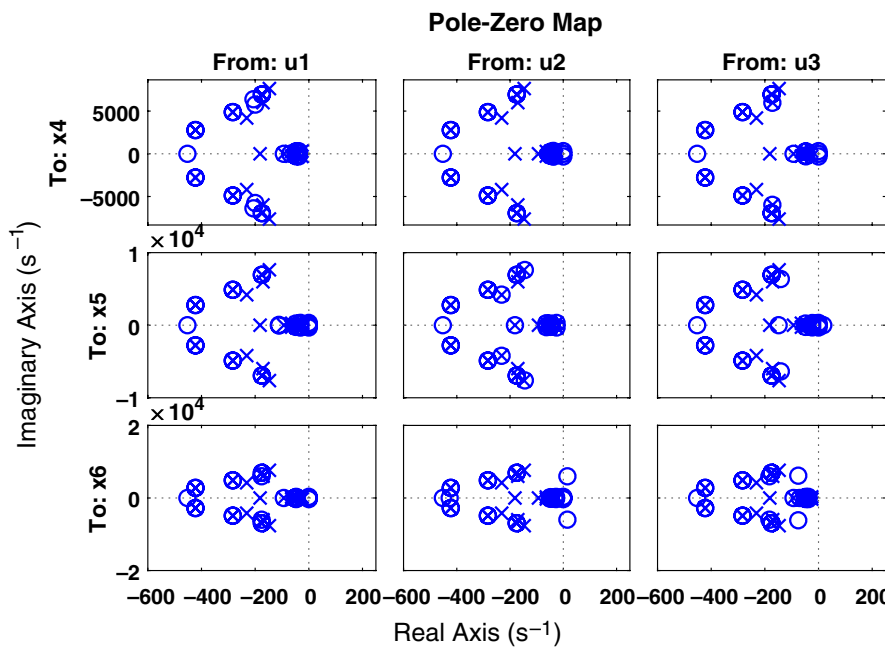
FIGURE 6 Inner-loop step responses

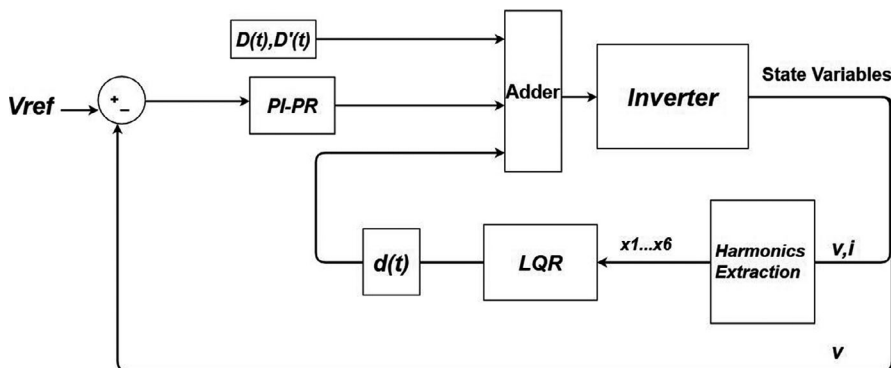**FIGURE 7** Poles and zeros map of closed-loop system

FIGURE 8 Block diagram of nested control loop

**TABLE 1** Parameters of the inverter

Parameters	Values
Vo_{ref}	$311\sin(\omega t)$
C_1, C_2	100 μF
L_1, L_2	100 μH
V_{in}	100 V
f_s	20 KHz
R_{Load}	$R = 100\ \Omega$
L_{Load}	$L = 30\ mH$

5 | SIMULATION RESULTS

The performance of the proposed nested control loop in the problem of overall behavior improvement and reference voltage tracking has been tested through simulation by using MATLAB/Simulink software. In this section, to evaluate the performance of the closed-loop system, a designed nested
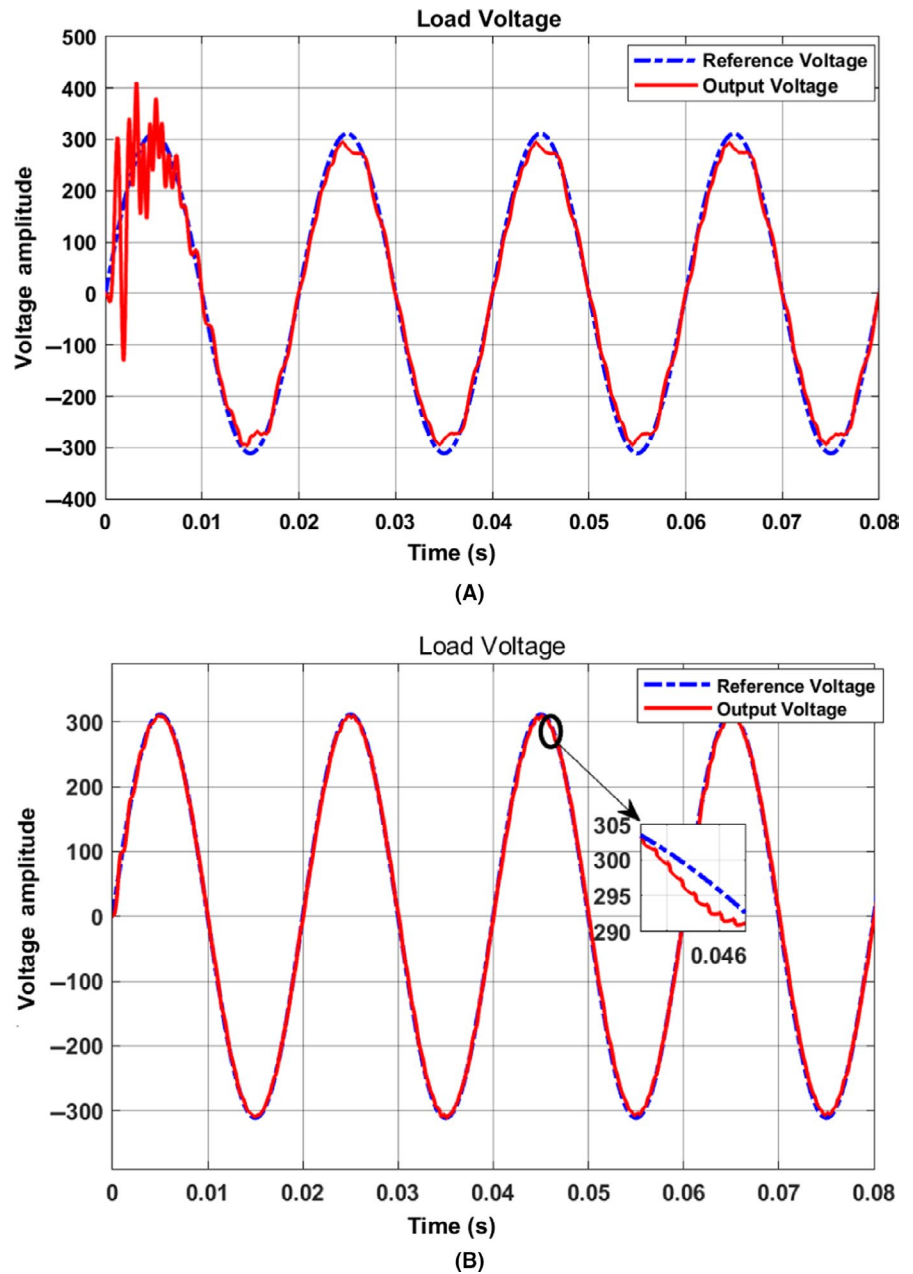
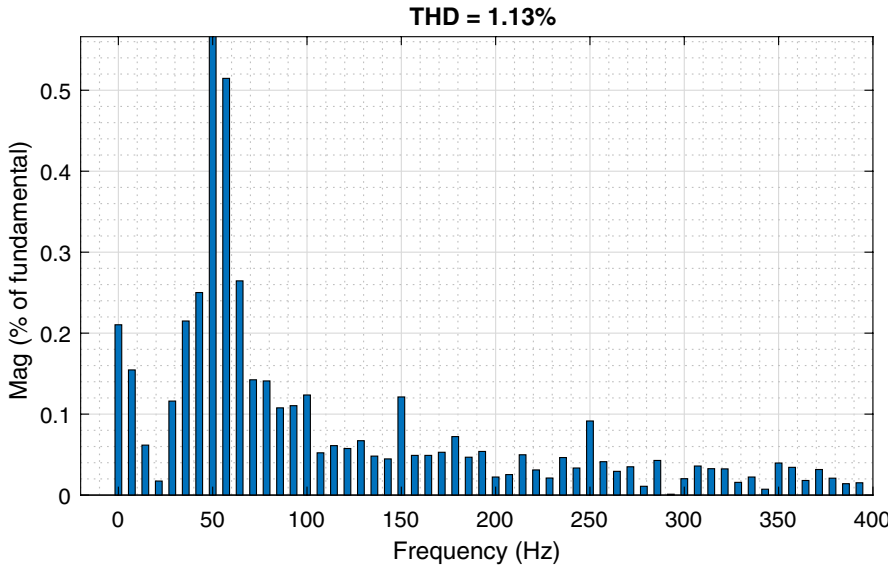**FIGURE 9** Output voltage of DBI with inductive load, A, open loop, B, closed loop

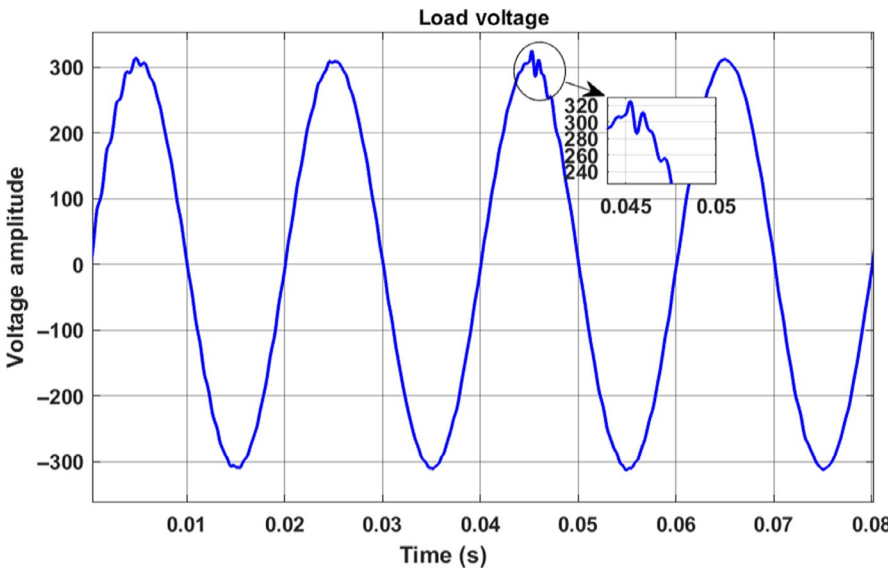**FIGURE 10** Voltage THD of closed-loop system with inductive load

FIGURE 11 Inductive load voltage of closed-loop system while input voltage is changed from 100 to 80 V at second 0.045
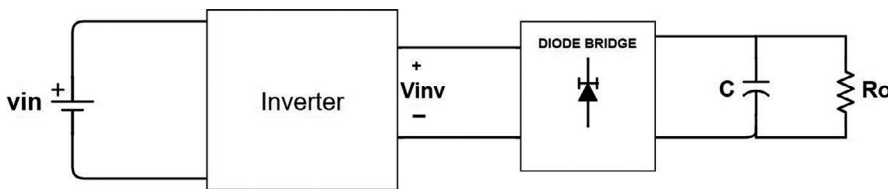

**FIGURE 12** Circuit diagram of DBI with nonlinear load

control loop is applied to full circuit Figure 2. The voltage references and inverter parameters are given in Table 1.

The optimal feedback gain of the inner control loop is designed to provide enough damping to improve the transient state of the output voltage. The PI-PR controller of outer control loop is calculated by trial and error $(K_p = 0.0037, K_i = 0.00015, K_r = 0.00001)$ to track desired

voltage accurately and reject disturbances. Nominal performances of DBI are illustrated in Figure 9.

As can be seen in Figure 9A, the load voltage of the open-loop system has extreme oscillations in transient state and steady state while Figure 9B shows the nested control loop strategy provides enough damping to eliminate extreme oscillations in transient the transient state. Also, as it is seen in

FIGURE 13 Output voltage of DBI with nonlinear load
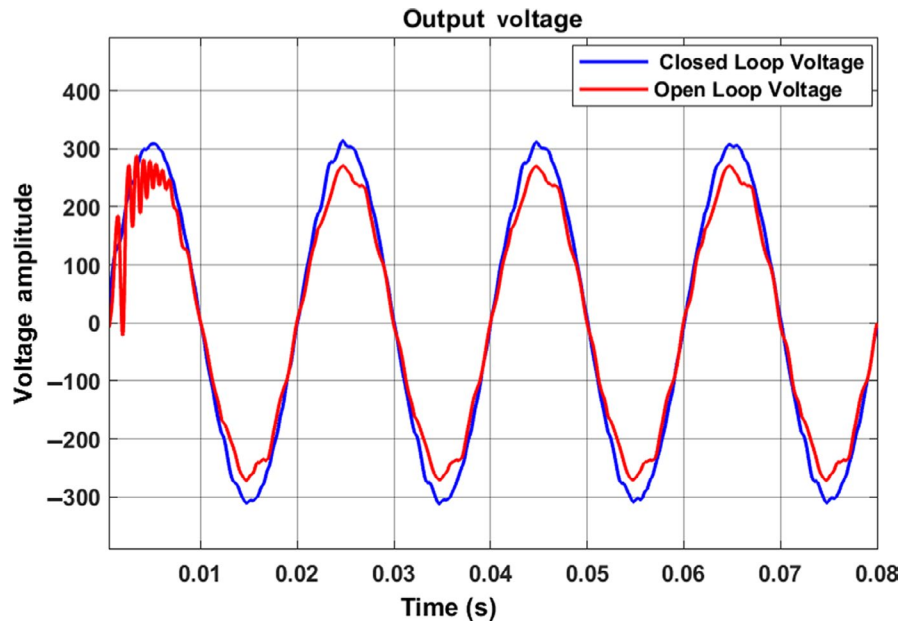
the magnified axes, the steady-state error is under 1.5% of reference voltage.

According to Figure 9, the closed-loop system provides overall behavior improvement due to both control loop performances. In fact, while the first loop increases damping and improves transient state, the outer loop tries to improve steady state by tracking the desired voltage. The corresponding THD is attained about 1.13% for an inductive load that is in the standard interval (based on the requirement of IEEE 1547 standard (THD < 5%)). The THD bar chart is shown in Figure 10 for inductive load.

In the following, to examine controlled inverter in photovoltaic panel shading condition, the inverter with nested control loop is tested by applied step disturbance (20% of input voltage) to the input voltage. The load voltage has been shown in Figure 11

In Figure 12, when input voltage decreases from 100 to 80 V at second 0.045, some oscillations can be seen as input voltage reduction effect which this effect is eliminated by nested control loop immediately and DBI can track the reference voltage with the lower input voltage.

The DBI is also tested with a nonlinear load, as is shown in Figure 12. Figure 13 shows the inverter voltage. Ro and C values are 170 Ω and 65 μF, respectively. In this test, the proposed control loop strategy shows a good performance in dealing with nonlinear load and THD of inverter voltage is attained about 1.74%.

Figure 14 shows the performance of closed-loop system while circuit parameter values (L, C) are changed.

Figure 14 shows some fluctuation when inductor values are changed from 100 to 145 μH and capacitor values are

changed from 100 to 170 μF at second 0.045 and track desired voltage instantly.

To evaluate the proposed nested control loop strategy, the sliding mode controller (SMC) that designed in[9] is applied as well. The sliding mode control uses a sliding surface that is a linear combination of inductor current and capacitor voltage errors, with coefficients k_1 and, k_2 , respectively. In consequence, this surface generates the switching pulses via a hysteresis comparator which causes some problems such as variable switching frequency. Another disadvantage of this method is instability in dealing with some external disturbances. Although the SMC nominal simulation result is similar to the proposed control strategy, but nested control loop provides higher robustness in dealing with applied disturbances. Figure 15 shows the performance of closed-loop system with nested loop control strategy when a square waveform with a 20% amplitude of input voltage and 100 Hz frequency applied to input voltage as an external disturbance. In fact, the key parameters of square wave disturbance in this paper are having higher order harmonics which is more challenging than a simple step. Also, it is shown our nested control loop can be stable while this disturbance entered to system with higher frequency than output voltage. As can be seen in Figure 15A, the inverter with the proposed control strategy remains stable in dealing with an external disturbance while in Figure 15B the inverter the SMC technique becomes unstable.[9] In addition, the THD of the closed-loop system with the proposed technique in this situation is attained about 2.95%.
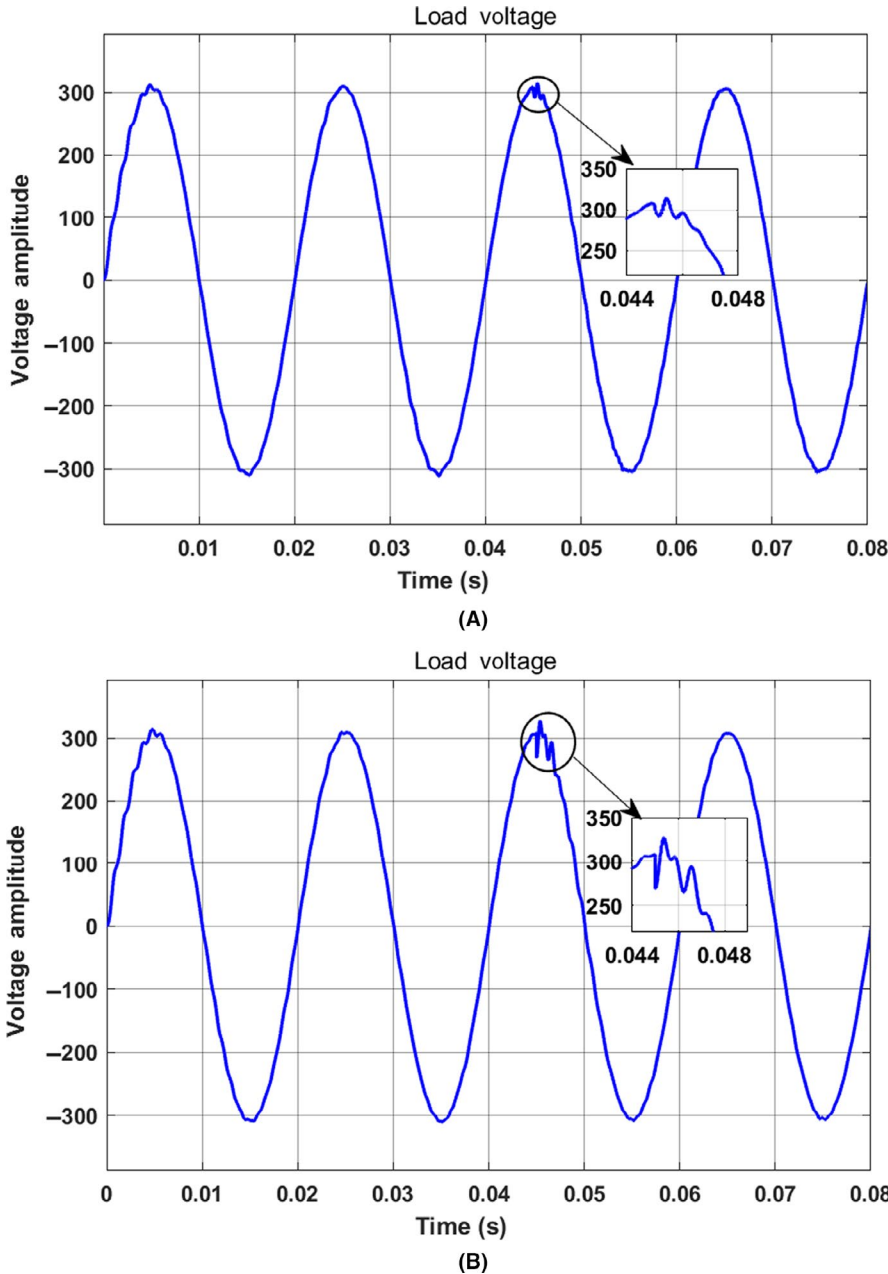
FIGURE 14 Inductive load voltage of closed-loop system while inductors and capacitors values are changed from (A) 100 to 145 μH and (B) 100 to 170 μF at second 0.045

6 | CONCLUSION

To transmit photovoltaic energy to a single phase local AC load, a voltage source inverter has been proposed and studied. Due to the inherent nonlinearity and in order to variable operation point condition of both boosts, a modeling method so-called GAM is proposed to achieve a LTI model. A nested control loop method is proposed in which both boost converters are controlled by means of a double-loop control structure. The inner loop uses an optimal state feedback controller which is designed based on LQR theory and GAM method to increase system damping, and a PI-PR controller is used as an outer loop controller to track desired voltage and reject disturbances. To evaluate the performance of the proposed control strategy, the nested control loop structure is compared to the sliding mode controller. The nominal linear load performance of both control schemes is similar. However, as it is shown in simulation results, the DBI with the SMC technique is unstable in dealing with some disturbances and the output voltage of inverter reaches to impossible value. Overall, the nested control loop performance shows good results under difficult situations such as dealing with nonlinear load, applied external disturbances in input voltage, and parameter values variations which in all of those situations the THD is attained under 3%.

FIGURE 15 Inductive load voltage of closed-loop system with (A) nested control loop (B) SMC technique[9] while square waveform with 20% amplitude of input voltage and 100 H frequency applied to input voltage as external disturbance

(A)

(B)

ORCID

Ali Amirparast 🆔 https://orcid.org/0000-0003-3812-6488
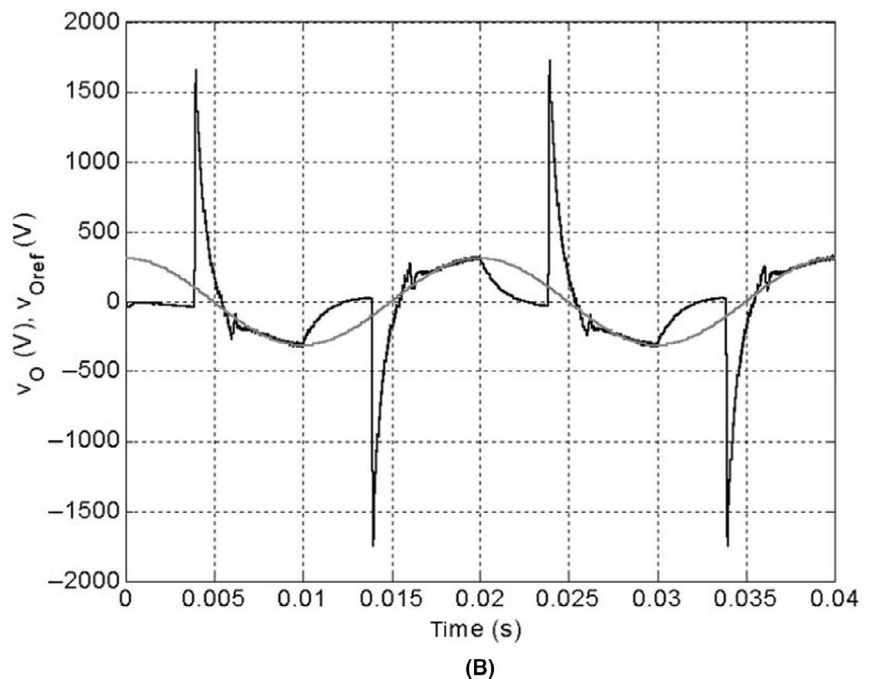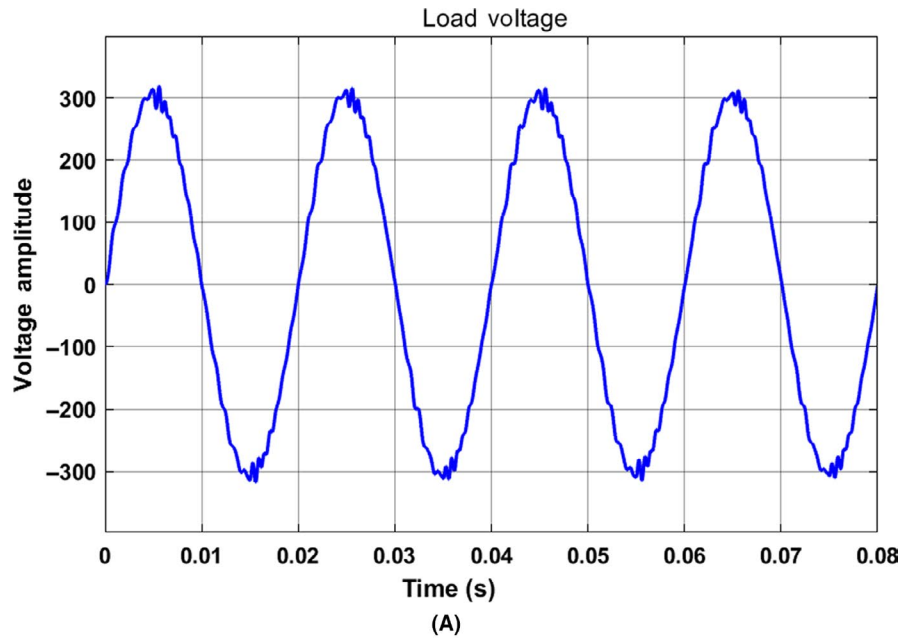
REFERENCES

1. Ahmadi MH, Ghazvini M, Sadeghzadeh M et al Solar power technology for electricity generation: a critical review. *Energy Sci Eng*. 2018;6(5):340-361.
2. Summer L, Fritz C, Vincent C et al Design, operation, and performance evaluation of a cable-drawn dual-axis solar tracker compared to a fixed-tilted system. *Energy Sci Eng*. 2015;3(6):549-557.
3. Ahmed I, Al-Emadi N, Gastli A, Ben-Brahim L. Mitigation of voltage imbalance in power distribution system using MPC-controlled packed-U-cells converter. *Energy Sci Eng*. 2019;7(5):1659-1668.
4. Caceres RO, Barbi I. A boost dc-ac converter: analysis, design, and experimentation. *IEEE Trans Power Electron*. 1999;14(1):134-141.
5. Kazimierczuk MK. Synthesis of phase-modulated resonant dc/ac inverters and dc/dc convertors. *IEE Proc B - Electric Power Appl*. 1992;139(4):387-394.
6. Caceres R, Barbi I. Sliding mode controller for the boost inverter. In V IEEE International Power Electronics Congress Technical Proceedings, CIEP 96, Oct 1996:247-252.
7. Dixon L. Average current mode control of switching power supplies. In Unitrode Power Supply Design Sem. (SEM700), 1990.
8. Naim R, Weiss G, Benyaakov S. H infinity control applied to boost power converters. *IEEE Trans Power Electron*. 1997;12:677-683, 08.
9. Sanchis P, Ursaea A, Gubia E, Marroyo L. Boost dc-ac inverter: a new control strategy. *IEEE Trans Power Electron*. 2005;20(2):343-353.

10. Liu J, Yin Y, Luo W, Vazquez S, Franquelo LG, Wu L. Sliding mode control of a three-phase ac/dc voltage source converter under unknown load conditions: Industry applications. *IEEE Trans Syst Man Cybernetics: Syst*. 2018;48(10):1771-1780.

11. Yin Y, Liu J, Sanchez JA et al Observer-based adaptive sliding mode control of NPC converters: an RBF neural network approach. *IEEE Trans Power Electron*. 2019;34(4):3831-3841.

12. Vazquez N, Alvarez J, Aguilar C, Arau J. Some critical aspects in sliding mode control design for the boost inverter. In 6th IEEE Power Electronics Congress. Technical Proceedings. CIEP 98 (Cat. No.98TH8375), Oct 1998:76-81.

13. Huang S, Tang F, Xin Z, Xiao Q, Loh PC. Grid-current control of a differential boost inverter with hidden lcl filters. *IEEE Trans Power Electron*. 2018:889-903, 03.

14. Abou-Kandil H, Freiling G, Ionescu V, Jank G. *Matrix Riccati Equations in Control and Systems Theory*. 1st ed. Basel, Switzerland: Birkhäuser Basel; 2003:257-297.

15. Ngamkong P, Kochcha P, Areerak K, Sujitjorn S, Areerak K. Applications of the generalized state-space averaging method to modelling of dc-dc power converters. *Math Comput Model Dyn Syst*. 2012;18(3):243-260.

16. Seddik B, Munteanu I, Bratcu A. *Power Electronic Converters Modeling and Control with Case Studies*. London, UK: Springer-Verlag; 2013:98-112, 09.

17. Maciejowski J. *Multivariate Feedback Design*. 1st ed. Boston, MA: Addison-Wesley Educational Publishers Inc; 1989:210-217, 01.

18. Subbaram Naidu D. *Optimal Control Systems*. 1st ed. Boca Raton, FL: CRC Press, N.W. Corporate Blvd.; 2002:108-118.

19. Masoud Karimi S, Khajehoddin A, Jain P, Bakhshai A. Linear quadratic output tracking and disturbance rejection. *Int J Control*. 2011;84(8):1442-1449.

20. Nowak M, Pirog S. Simulation studies of the proportional resonant controller. *Przeglad Elektrotechniczny*. 2018;94:128-131, 06.